# High-resolution Auger spectroscopy of Na-like argon and sulfur ions singly excited in high-energy collisions with light target atoms

I. Kádár,* H. Altevogt, R. Köhrbrück, V. Montemayor,† A. Mattis, G. Schiwietz, B. Skogvall, K. Sommer, and N. Stolterfoht‡
*Hahn-Meitner Institut Berlin GmbH, Glienicker Strasse 100, D-1000 Berlin 39, Germany*

K. Kawatsura
*Kyoto Institute of Technology, Matsugasaki, Sakyoku, Kyoto 606, Japan*

M. Sataka, Y. Nakai, and H. Naramoto
*Department of Physics, Japan Atomic Energy Research Institute, Tokai, Ibaraki 319-11, Japan*

Y. Kanai, T. Kambara, and Y. Awaya
*Institute of Physical and Chemical Research (RIKEN), Wako, Saitama 351-01, Japan*

K. Komaki and Y. Yamazaki
*Institute of Physics, College of Arts and Sciences, University of Tokyo, Meguro, Tokyo 153, Japan*
(Received 11 December 1990)

Singly excited states of sodiumlike argon and sulfur have been investigated by means of high-resolution 0° Auger spectroscopy at high projectile energies. The Auger-electron spectrum is due to the decay of states populated by monopole, dipole, and quadrupole excitation of the $2p$ and $2s$ electrons. Collision strengths calculated by means of the configuration-interaction Hartree-Fock program by Cowan [*The Theory of Atomic Structure and Spectra* (University of California Press, Berkeley, 1981)] in the plane-wave Born approximation (PWBA) have been used to describe the relative intensities found in the measured spectrum. The intensities due to monopole excitation are significantly higher than the prediction by PWBA for a Coulomb perturbation potential. The structure of the emitted electron spectrum is found to be significantly influenced by the configuration interaction.

## INTRODUCTION

The technique of 0° projectile Auger spectroscopy [1,2] is a powerful tool for the high-resolution study of the structure of highly charged projectile ions. Moreover, using swift projectiles and a light gas target this method allows for the study of selectively excited configurations and thereby also that of specific excitation mechanisms [2,3]. Usually the light target atom interacts only with one electron of the projectile ion leaving the others unchanged. Consequently, under single-collision conditions the collision with a projectile ion of properly chosen charge state results in a few selected excited states.

In this work we deal with the $L$ Auger electrons emitted by high-energy sodiumlike projectiles excited by light target atoms. The level diagram of the sodiumlike $Ar^{7+}$ ion is shown in Fig. 1. The ground state is $1s^2 2s^2 2p^6 3s\ ^2S_{1/2}$. The only configurations which can decay by the emission of an $L$ Auger electron are those in which there are at least two electrons in levels with $n \geq 2$ in addition to the $L$-shell vacancy. At high projectile energies the energy spectrum of Auger electrons emitted in collisions of a Na-like ion with a He atom is composed mainly of transitions from singly excited initial states. It is noted that single ionization does not yield autoionizing states. Double ionization of the $L$ shell, excitation, or ionization events with an accompanying additional excitation could in principle produce autoionizing states. In the present collision system, however, the light He target ensures that the contribution of multiple electron excitation and/or ionization events in one collision are negligible. Single ionization of the $K$ shell produces an autoion-

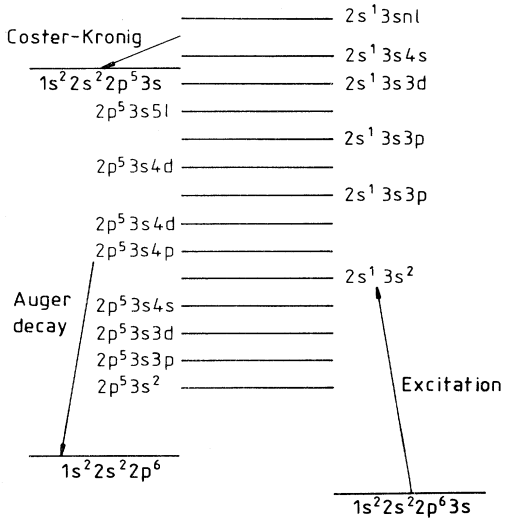


FIG. 1. Level diagram for the excitation and decay of the $Ar^{7+}$ ion.

 

izing state, but the corresponding cross section is significantly smaller than that for the $L$ shell. Accordingly, most of the Auger lines found in the spectrum originate from levels populated by single excitation events. The resulting Auger-electron spectrum is relatively simple, especially because only one final state, the neonlike $1s^2 2s^2 2p^6\ ^1S_0$, is relevant for the Auger decay. Beside the study of the structure of these interesting open-shell ions, the high-resolution measurement of these spectra also enables the investigation of the excitation mechanism. A practical advantage of the sodiumlike projectiles is that there is no metastable component in the beam.

In recent years a number of different authors have dealt with Na-like heavy ions. In most of the cases [4–8] the excited Na-like ions were produced by electron capture using a slow heavy-ion beam. The resulting spectrum is rather complicated because many levels are populated by the capture. A study of singly excited Na-like Ti has been performed by Schneider *et al.* [9] with moderate energy resolution using 3.4-MeV/u Na-like Ti projectiles excited by a He target. Although most of the lines were not resolved, i.e., no real structure information could be obtained from this measurement, it was clearly observed that the main features of the spectrum are due to levels populated by monopole, dipole, and quadrupole excitations of the $2p$ subshell electrons. These conclusions were drawn from comparing the observed spectrum with theoretical data.

In the following a high-resolution study of singly excited Na-like argon and sulfur is presented. The aim of this study is to obtain more detailed information on the excitation mechanism as well as on the structure of different excited Na-like ions. A model spectrum was constructed, based on transition energies, transition rates, and collision strengths calculated by using the multiconfiguration configuration-interaction Hartree-Fock (CIHF) code by Cowan [10]. Information on both structure and collision mechanisms could be drawn from the comparison of this model with the measured $L$ Auger spectrum.

## EXPERIMENT

The experiments with a beam of 2.75-MeV/u (110-MeV) $Ar^{7+}$ ions were performed at the VICKSI accelerator facility of the Hahn-Meitner Institut in Berlin. The measurements using 2-MeV/u (64-MeV) $S^{5+}$ beams were realized at the tandem accelerator of the Japan Atomic Energy Research Institute in Tokai, Japan. The well-collimated ( $<3\times3$ mm$^2$) beam passed through a gas cell and the first stage of a tandem parallel-plate electron spectrometer [2]. This spectrometer was used to measure the energy spectrum of the electrons emitted in the direction of the beam. The first of the two 45° parallel-plate spectrometers mounted in series was used as a deflector, merely deflecting the electrons out of the beam direction, thereby facilitating their energy analysis by the second parallel-plate condenser. The tandem spectrometer has been described in detail elsewhere [2].

The high resolution necessary for these measurements was achieved by decelerating the electrons before the energy analysis. In the case of the $Ar^{7+}$ measurements the deceleration was performed in two steps. First, prior to entering the tandem spectrometer, the electrons were decelerated by a constant positive voltage applied to the gas cell. The electrons were further decelerated after the first (deflecting) condenser before entering the second (analyzing) spectrometer. This latter spectrometer worked in the constant-pass-energy mode, ensuring constant energy resolution, which facilitates the evaluation procedure. In conjunction with the $S^{5+}$ measurements only the second deceleration step was used.

For making the first deceleration step feasible, one should be able to bias electrically the body of the gas cell also when it is under pressure. To avoid discharges in the gas inlet system of the cell, a particular gas inlet system has been constructed. It consists of a long insulating tube followed by a metallic flow resistance tube in electrical contact with the body of the cell. The pressure in the plastic inlet tube is a few hundred mbar at normal working pressures of the cell and it changes from this value to the cell pressure (around 0.1 mbar) inside the conducting flow resistance tube. This way the pressure region, where electrical discharges are probable, is at the same high potential inside the flow resistance tube as the gas cell itself. This arrangement effectively prevents the discharges in the gas inlet system. The intensity loss due to angular magnification by the first deceleration step is partly compensated for by a negatively biased focusing lens positioned in the path of this first deceleration.

The acceptance angle of the spectrometer did not exceed 1° for electrons leaving the gas cell. This fact in addition to the good collimation of the ion beam kept the Doppler broadening of the Auger lines at about the same value as the instrumental resolution of the electron spectrometer.

## DATA EVALUATION

The measured electron spectra were decomposed by using the method of least squares, by fitting a sum of Gaussian peaks superimposed on a linear background to the spectrum. At the constant pass energy used in the measurements the experimental resolution was mainly determined by the instrumental width (at about 3% of the pass energy in the second stage of the analyzer in our case). This is why a single linewidth was used for all the measured peaks.

The energy positions of the lines have been found by transforming the spectra measured in the laboratory frame to the projectile frame taking into account relativistic effects. The projectile velocity (the cusp energy) used in the transformation was determined from the requirement that the experimental Auger energy transformed to the projectile frame should be independent of the direction of the electron emission, i.e., whether this energy was determined from the laboratory frame energy of the forward or backward emitted Auger electrons [3]. This method cancels in first order uncertainties such as contact potential which influences the cusp energy determination.

The accuracy of our energy scale has been verified by

TABLE I. Experimental Auger-electron energies for the $1s^2 2s^2 2p^5 3s^2\,{}^2P_J - 1s^2 2s^2 2p^6$ transitions in $Ar^{7+}$.

| | Auger energy (eV) | | | |
|---|---|---|---|---|
| Term | Present | Hutton *et al.*[a] | Bordenave-Montesquieu *et al.*[b] | Matsuo *et al.*[c] |
| $^2P_{3/2}$ | 100.6±0.2 | 100.6±0.33 | 100.1±0.3 | 100.3±0.2 |
| $^2P_{1/2}$ | 102.7±0.2 | 102.8±0.33 | 102.6±0.3 | 102.7±0.2 |

[a]Reference [4].
[b]Reference [5].
[c]Reference [11].

comparing our values with the experimental energy values determined by others. Experimental energies are available [4,5,11] for the case of the $1s^2 2s^2 2p^5 3s^2\,{}^2P_J - 1s^2 2s^2 2p^6$ transitions in $Ar^{7+}$. The latter experimental energies agree with our experimental values to within the experimental error as shown in Table I.

For facilitating the identification of the spectral lines the spectrum obtained has been modeled by utilizing the CIHF code by Cowan [10]. Making use of the possibilities given by this program both the energy values and the expected relative transition intensities (excitation and decay probabilities) were calculated by using the same HF wave functions. The model calculations have been performed by taking into account the interaction between all the relevant configurations as follows (completely filled subshells are omitted to facilitate the notation): (1) $2p^5 3sns$, $2p^5 3snd$ ($n=3,4,5$), $2p^5 3p^2$, $2p^5 3d^2$, $2s^1 2p^6 3s 3p$; (2) $2p^6 3s$, $2p^5 3snp$, $2s^1 3sns$, $2s^1 3snd$ ($n=3,4,5$); and (3) $2s^1 2p^6 3snp$ ($n=3,4$), $2p^5 3sns$, $2p^5 3snd$ ($n=3,4,5$).

Radiative transition probabilities have been computed taking into account only electric dipole transitions to all the lower lying levels of appropriate parity.

Collision strengths calculated in the plane-wave Born approximation by using also the CIHF code by Cowan [10] have been used to describe the relative intensities found in the measured spectrum. The collision strengths were calculated taking into account the interaction between the same configurations as in the case of the energy determination.

The population of the excited states can be estimated in two different ways. One possibility is to estimate the population of the states produced by dipole and quadrupole excitation of the $L$ electrons by high-energy light projectiles by the corresponding oscillator strengths, since the Coulomb field of the target in these high speed collisions resembles an impinging photon. This estimation does not give account of the population of states produced by monopole excitation.

A better estimate of the measured spectrum is the collision strength $\Omega$ which has been calculated by the same CIHF code of Cowan [10] for a high-energy (100 times threshold energy) electrons in the plane-wave Born approximation (PWBA). The collision strength is defined by

$$\Omega_{JJ'}(\varepsilon) \equiv (E_{J'} - E_J) g Q_{JJ'}(\varepsilon) = \frac{8\pi}{\varepsilon} \int_{K_{\min}}^{K_{\max}} g f_{JJ'}(K) d(\ln K) .$$

Here $g$ is the statistical weight of the initial state ($g=2J+1$), $\varepsilon = k^2 \geq \Delta E$ the initial electron energy, $Q_{JJ'}$ the total cross section in $a_0^2$ units, $f_{JJ'}(K)$ the generalized oscillator strength [12], $K$ the momentum transfer, and $k$ the momentum of the free electron:

$$g f_{JJ'} = \frac{E_{J'} - E_J}{K^2} \times \sum_t (2t+1) \left\langle \gamma J \left| \left| \sum_m j_t(K r_m) C_m^{(t)} \right| \right| \gamma' J' \right\rangle^2$$

where $t$ is the angular momentum transfer, $j_t(K r_m)$ the Bessel function of order $t$, $m$ the index for the active electron under consideration, $r_m$ its position vector, and $C_m^{(t)}$ the renormalized spherical harmonics.

The Auger spectrum intensity distribution is approximated by

$$I_{J'} = \frac{\Omega_{JJ'}(\varepsilon)}{(E_{J'} - E_j) g} A_{J'} .$$

The transitions are classified according to the multipole expansion of the plane wave in the PWBA description. A transition with a given angular momentum transfer is described by the corresponding multipole matrix elements containing the Bessel function of appropriate order. In the following the concept of multipole transitions will be used in this sense. Since the zeroth-order Bessel function differs from zero, the PWBA multipole description also characterizes monopole transitions unlike the optical multipole case. The configurations populated in the collisions by single excitation differ only in the quantum numbers of one electron from the ground state of the ion. Since the ground state of the sodiumlike ions is a $^2S_{1/2}$ state, the different singly excited ionic states are created by one-electron excitation with a single angular momentum transfer. Accordingly only one multipole matrix element is required to describe the excitation of a specific state.

The calculations have been performed for monopole, dipole, and quadrupole excitation. Higher-order multipole excitation modes do not give a significant contribution. Because of the small mass of the electron and the

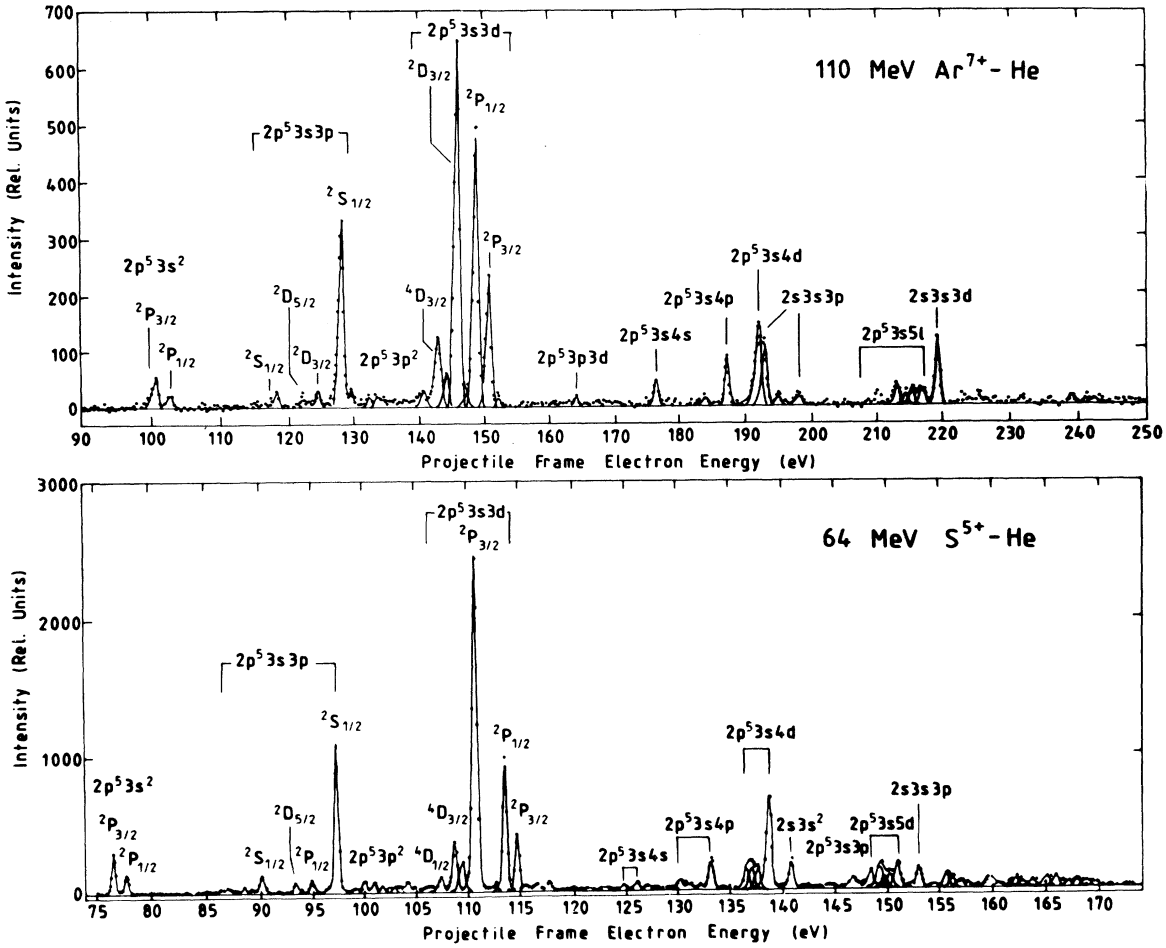


FIG. 2. Energy spectra of the $L$ Auger electrons emitted in the 110-MeV $Ar^{7+}$-He (a) and 64-MeV $S^{5+}$-He (b) collisions. Energy values are given in the projectile frame.

lack of screening the Auger spectrum estimated in this manner can reproduce only the relative intensity values in the spectrum, but not the absolute cross sections.

## RESULTS AND DISCUSSION

The energy spectrum of $L$ Auger electrons obtained in 110-MeV $Ar^{7+}$-He collisions by the excitation of $L$-shell electrons is shown in Fig. 2(a), while that for the 64-MeV $S^{5+}$-He collision is shown in Fig. 2(b). The lines found in the experimental spectrum were assigned to the corresponding Auger transitions using the theoretical transition energies and their differences as well as the relative intensities calculated by the Cowan CIHF code [10]. The identification of the measured electron lines as well as the calculated and measured energy and intensity values for the $Ar^{7+}$ and $S^{5+}$ projectiles are shown in Tables II and III, respectively.

The strongest argument for the assignment was always the energy of the given line. According to the assignments the most prominent groups of lines are those due to the decay of $2p^53s^2$, $2p^53s3p$, and $2p^52s3d$ configurations to the neonlike $1s^22s^22p^6$ configuration, which is the only possible final state for the Auger transitions. The other groups shown at higher electron energies are Auger electrons originating from the $2p^53snl$ configurations ($n > 3$), as well as those from $2s^12p^63s3l$. Most of the lines originating from the $2p^53s3l$ configurations are well resolved, while those involving electrons with $n > 3$ are not always separated experimentally. The same is true for the lines due to Auger transitions from configurations having a $2s$ hole instead of the $2p$ one.

At this high projectile velocity the cross section for populating states by lifting a $2s$ electron to a higher bound state is expected to be smaller than the corresponding cross section for the excitation of a $2p$ electron, since the $2s$ binding energy is higher than that of $2p$ electrons and the number of electrons is higher by a factor of 3 in the $2p$ subshell. This is why the population of the $2s^13snl$ configurations is generally smaller than that for $2p^53snl$.

The spectrum of Auger electrons emitted in 64-MeV $S^{5+}$-He collisions differs from those obtained in 110-MeV $Ar^{7+}$-He collisions. Differences occur primarily in the relative energy position of the lines due to transitions from levels originating from the excitation of the $2p$ and $2s$ electrons, respectively. The contribution of the Auger

TABLE II. Experimental and theoretical energies and relative intensities of the Auger electrons emitted in the 110-MeV $Ar^{7+}$-He collisions. Theoretical values are calculated using the CIHF program by Cowan [10]. Both the theoretical and experimental total intensities are normalized to 1000. States with a theoretical Auger intensity expectation less than 0.5 are omitted. The common final state of all of the transitions is $1s^2 2s^2 2p^6\,{}^2S_0$.

| | Auger energy | | Intensity | |
|---|---|---|---|---|
| Initial state | Expt. | Theory | Expt. | Theory |
| $2p^5 3s^2\,{}^2P_{3/2}$ | 100.6 | 100.18 | 16.3 | 21.99 |
| $2p^5 3s^2\,{}^2P_{1/2}$ | 102.7 | 102.31 | 7.4 | 11.56 |
| $2p^5 3s(^3P)3p\,{}^4D_{3/2}$ | | 114.46 | | 0.54 |
| $2p^5 3s(^3P)3p\,{}^4P_{5/2}$ | | 115.43 | | 1.24 |
| $2p^5 3s(^3P)3p\,{}^4P_{3/2}$ | | 115.70 | | 1.80 |
| $2p^5 3s(^1P)3p\,{}^2D_{3/2}$ | | 116.86 | | 1.91 |
| $2p^5 3s(^1P)3p\,{}^2D_{5/2}$ | | 117.49 | | 4.97 |
| | 118.2 | | 8.1 | |
| $2p^5 3s(^1P)3p\,{}^2S_{1/2}$ | | 118.54 | | 1.65 |
| $2p^5 3s(^3P)3p\,{}^2D_{5/2}$ | 122.2 | 122.66 | 6.2 | 1.68 |
| $2p^5 3s(^3P)3p\,{}^2D_{3/2}$ | | 125.10 | | 0.75 |
| | 124.6 | | 9.5 | |
| $2p^5 3s(^3P)3p\,{}^2P_{1/2}$ | | 125.17 | | 1.19 |
| $2p^5 3s(^3P)3p\,{}^2S_{1/2}$ | 128.2 | 129.88 | 115.4 | 42.90 |
| $2p^5 3p(^1D)3p\,{}^2P_{1/2}$ | | 132.39 | | 1.99 |
| | 132.3 | | 7.4 | |
| $2p^5 3p(^1D)3p\,{}^2P_{3/2}$ | | 132.64 | | 2.06 |
| $2p^5 3p(^3P)3p\,{}^4P_{3/2}$ | 133.3 | 133.36 | 8.0 | 1.03 |
| $2p^5 3p(^1S)3p\,{}^2P_{3/2}$ | | 140.04 | | 3.41 |
| | 140.6 | | 10.8 | |
| $2p^5 3p(^1S)3p\,{}^2P_{1/2}$ | | 141.13 | | 1.70 |
| $2p^5 3s(^3P)3d\,{}^4D_{1/2}$ | | 142.65 | | 15.11 |
| | 142.7 | | 47.0 | |
| $2p^5 3s(^3P)3d\,{}^4D_{3/2}$ | | 142.79 | | 26.18 |
| $2p^5 3s(^1P)3d\,{}^2P_{3/2}$ | | 143.57 | | 2.02 |
| $2p^5 3p(^1S)3p\,{}^2P_{1/2}$ | | 143.86 | | 0.90 |
| $2p^5 3s(^1P)3d\,{}^2D_{3/2}$ | 144.0 | 144.03 | 23.6 | 2.31 |
| $2p^5 3s(^1P)3d\,{}^2P_{3/2}$ | | 146.22 | | 242.87 |
| | 145.9 | | 235.1 | |
| $2p^5 3s(^1P)3d\,{}^2P_{1/2}$ | | 146.33 | | 103.74 |
| $2p^5 3s(^3P)3d\,{}^2D_{3/2}$ | | 148.78 | | 40.59 |
| | 148.8 | | 182.9 | |
| $2p^5 3s(^3P)3d\,{}^2P_{1/2}$ | | 149.30 | | 86.68 |
| $2p^5 3s(^3P)3d\,{}^2P_{3/2}$ | 150.7 | 150.81 | 82.8 | 93.17 |
| $2p^5 3s(^3P)4s\,{}^2P_{3/2}$ | 176.6 | 177.58 | 14.8 | 2.14 |
| $2p^5 3s(^1P)4s\,{}^2P_{3/2}$ | | 178.66 | | 0.64 |
| $2s^1 3s(^2S)3s\,{}^2S_{1/2}$ | | 180.03 | | 3.54 |
| $2p^5 3s(^3P)4p\,{}^4P_{1/2}$ | | 184.15 | | 0.54 |
| $2p^5 3s(^3P)4p\,{}^2S_{1/2}$ | 187.3 | 188.62 | 27.5 | 14.05 |
| $2p^5 3s(^3P)4d\,{}^2D_{3/2}$ | | 191.83 | | 1.52 |
| $2p^5 3s(^1P)4d\,{}^2P_{1/2}$ | | 192.13 | | 2.41 |
| $2p^5 3s(^3P)4d\,{}^4D_{1/2}$ | | 192.35 | | 17.49 |
| $2s^1 3s(^3S)3p\,{}^4P_{1/2}$ | | 192.59 | | 0.98 |
| $2s^1 3s(^3S)3p\,{}^4P_{3/2}$ | 192.0 | 192.67 | 53.7 | 1.84 |
| $2p^5 3s(^3P)4d\,{}^4D_{3/2}$ | | 192.84 | | 26.07 |
| $2p^5 3s(^3P)4d\,{}^4F_{3/2}$ | | 193.79 | | 16.12 |
| $2p^5 3s(^1P)4d\,{}^2P_{3/2}$ | | 194.45 | | 6.92 |
| $2p^5 3s(^1P)4d\,{}^2P_{1/2}$ | 192.9 | 194.83 | 44.1 | 37.36 |
| $2p^5 3s(^1P)4d\,{}^2D_{3/2}$ | | 194.92 | | 42.33 |
| $2s^1 3s(^1S)3p\,{}^2P_{1/2}$ | | 196.58 | | 1.41 |
| | 195.0 | | 7.0 | |
| $2s^1 3s(^1S)3p\,{}^2P_{3/2}$ | | 196.68 | | 2.71 |

TABLE II. (*Continued*).

| Initial state | Auger energy | | Intensity | |
|---|---|---|---|---|
| | Expt. | Theory | Expt. | Theory |
| $2s^13s(^3S)3p\ ^2P_{1/2}$ | 198.1 | 202.41 | 7.0 | 1.42 |
| $2s^13s(^3S)3p\ ^2P_{3/2}$ | | 202.45 | | 2.26 |
| $2p^53s(^3P)5p\ ^4P_{1/2}$ | 213.1 | 210.77 | 16.7 | 1.27 |
| $2p^53s(^3P)5p\ ^2S_{1/2}$ | | 213.37 | | 5.14 |
| $2p^53s(^3P)5d\ ^2D_{3/2}$ | | 213.70 | | 3.95 |
| $2p^53s(^3P)5d\ ^2P_{1/2}$ | | 213.99 | | 11.07 |
| $2p^53s(^3P)5d\ ^2P_{3/2}$ | 215.4 | 214.61 | 13.8 | 14.63 |
| $2p^53s(^3P)5d\ ^4F_{3/2}$ | | 215.71 | | 6.58 |
| $2p^53s(^1P)5d\ ^2D_{3/2}$ | 217.0 | 216.73 | 14.4 | 14.34 |
| $2p^53s(^1P)5d\ ^2P_{1/2}$ | | 216.81 | | 11.55 |
| $2s^13s(^3S)3d\ ^2D_{5/2}$ | 219.4 | 221.93 | 40.7 | 14.16 |
| $2s^13s(^3S)3d\ ^2D_{3/2}$ | | 221.94 | | 9.49 |
| $2s^13s(^1S)4p\ ^2P_{3/2}$ | | 264.77 | | 0.54 |

TABLE III. Experimental and theoretical energies and relative intensities of the Auger electrons emitted in the 64-MeV $S^{5+}$-He collisions. Theoretical values are calculated using the CIHF code by Cowan [10]. Both the theoretical and experimental total intensities are normalized to 1000. States with a theoretical Auger intensity expectation less than 0.4 are omitted. The common final state of all of the transitions is $1s^22s^22p^6\ ^2S_0$.

| Initial state | Auger energy | | Intensity | |
|---|---|---|---|---|
| | Expt. | Theory | Expt. | Theory |
| $2p^53s^2\ ^2P_{3/2}$ | 76.7 | 75.49 | 24.8 | 28.72 |
| $2p^53s^2\ ^2P_{1/2}$ | 77.9 | 76.68 | 11.3 | 14.67 |
| $2p^53s(^3P)3p\ ^4P_{5/2}$ | 86.6 | 86.98 | 1.7 | 1.02 |
| $2p^53s(^3P)3p\ ^4P_{3/2}$ | | 87.21 | | 1.46 |
| $2p^53s(^1P)3p\ ^2D_{3/2}$ | 87.1 | 87.80 | 2.3 | 3.05 |
| $2p^53s(^1P)3p\ ^2D_{5/2}$ | 88.5 | 88.22 | 3.3 | 6.21 |
| $2p^53s(^1P)3p\ ^2S_{1/2}$ | 90.1 | 89.46 | 10.6 | 2.52 |
| $2p^53s(^3P)3p\ ^2D_{5/2}$ | 93.3 | 92.99 | 6.1 | 1.73 |
| $2p^53s(^3P)3p\ ^2D_{3/2}$ | | 93.56 | | 0.63 |
| $2p^53s(^3P)3p\ ^2P_{3/2}$ | 94.9 | 94.46 | 8.5 | 0.58 |
| $2p^53s(^3P)3p\ ^2P_{1/2}$ | | 94.62 | | 0.68 |
| $2p^53s(^3P)3p\ ^2S_{1/2}$ | 97.4 | 98.25 | 110.4 | 43.52 |
| $2p^53p(^1D)3p\ ^2P_{1/2}$ | 100.1 | 100.07 | 7.9 | 2.74 |
| $2p^53p(^1D)3p\ ^2P_{3/2}$ | 101.0 | 100.28 | 6.7 | 3.75 |
| $2p^53p(^3P)3p\ ^4P_{3/2}$ | | 100.80 | | 0.83 |
| $2p^53p(^1S)3p\ ^2P_{3/2}$ | 104.3 | 106.10 | 6.7 | 6.55 |
| $2p^53p(^1S)3p\ ^2P_{1/2}$ | 107.4 | 106.71 | 9.2 | 2.71 |
| $2p^53s(^3P)3d\ ^4D_{1/2}$ | | 107.69 | | 7.00 |
| $2p^53s(^3P)3d\ ^4D_{3/2}$ | 108.7 | 107.78 | 40.1 | 15.29 |
| $2p^53s(^3P)3d\ ^2D_{3/2}$ | | 108.49 | | 17.38 |

TABLE III. (*Continued*).

| Initial state | Auger energy | | Intensity | |
|---|---|---|---|---|
| | Expt. | Theory | Expt. | Theory |
| $2p^5 3s(^1P)3d\ ^2D_{3/2}$ | | 108.78 | | 5.16 |
| | 109.5 | | 19.5 | |
| $2p^5 3p(^1S)3p\ ^2P_{1/2}$ | | 108.86 | | 8.44 |
| $2p^5 3s(^3P)3d\ ^2P_{3/2}$ | | 110.05 | | 262.87 |
| | 110.7 | | 267.9 | |
| $2p^5 3s(^1P)3d\ ^2P_{1/2}$ | | 110.16 | | 128.58 |
| $2p^5 3s(^3P)3d\ ^2D_{3/2}$ | | 112.85 | | 16.29 |
| | 113.6 | | 95.0 | |
| $2p^5 3s(^3P)3d\ ^2P_{1/2}$ | | 113.25 | | 45.19 |
| $2p^5 3s(^3P)3d\ ^2P_{3/2}$ | 114.7 | 114.09 | 40.5 | 65.17 |
| $2p^5 3s(^1P)4s\ ^2P_{1/2}$ | | 125.30 | | 0.78 |
| | 124.7 | | 4.2 | |
| $2p^5 3s(^3P)4s\ ^2P_{3/2}$ | | 125.36 | | 3.58 |
| $2p^5 3s(^1P)4s\ ^2P_{3/2}$ | 126.0 | 126.10 | 5.4 | 0.44 |
| $2p^5 3s(^3P)4p\ ^2D_{5/2}$ | 130.2 | 129.93 | 9.4 | 0.41 |
| $2p^5 3s(^1P)4p\ ^2D_{5/2}$ | 131.0 | 131.14 | 5.4 | 0.41 |
| $2p^5 3s(^3P)4p\ ^2S_{1/2}$ | 133.1 | 133.23 | 25.9 | 11.12 |
| $2p^5 3s(^3P)4d\ ^4F_{3/2}$ | | 135.92 | | 3.21 |
| $2p^5 3s(^3P)4d\ ^2D_{3/2}$ | | 136.23 | | 0.85 |
| $2p^5 3s(^3P)4d\ ^2P_{1/2}$ | | 136.25 | | 18.15 |
| | 136.6 | | 19.7 | |
| $2p^5 3s(^3P)4d\ ^4D_{3/2}$ | | 136.51 | | 16.51 |
| $2p^5 3s(^3P)4d\ ^2P_{3/2}$ | 137.1 | 137.11 | 21.6 | 19.57 |
| $2p^5 3s(^1P)4d\ ^2P_{3/2}$ | 137.7 | 137.70 | 17.5 | 15.52 |
| $2p^5 3s(^1P)4d\ ^2D_{3/2}$ | | 138.02 | | 46.07 |
| | 138.7 | | 82.6 | |
| $2p^5 3s(^1P)4d\ ^2P_{1/2}$ | | 138.06 | | 36.32 |
| $2s^1 3s(^2S)3s\ ^2S_{1/2}$ | 140.8 | 143.44 | 23.3 | 5.37 |
| $2p^5 3s(^3P)5s\ ^2P_{3/2}$ | | 143.58 | | 0.51 |
| $2p^5 3s(^1P)5s\ ^2P_{3/2}$ | | 144.86 | | 0.40 |
| $2p^5 3s(^3P)5p\ ^2S_{1/2}$ | | 146.67 | | 0.71 |
| $2p^5 3s(^1P)5p\ ^2S_{1/2}$ | 146.7 | 148.41 | 8.7 | 10.87 |
| $2p^5 3s(^3P)5d\ ^2D_{3/2}$ | | 148.41 | | 5.82 |
| $2p^5 3s(^3P)5d\ ^2P_{1/2}$ | 148.5 | 148.59 | 14.5 | 14.13 |
| $2p^5 3s(^3P)5d\ ^4D_{3/2}$ | | 148.76 | | 0.43 |
| $2p^5 3s(^3P)5d\ ^4D_{1/2}$ | | 148.77 | | 0.69 |
| $2p^5 3s(^3P)5d\ ^4F_{3/2}$ | 149.3 | 148.97 | 21.3 | 16.88 |
| $2p^5 3s(^3P)5d\ ^2P_{3/2}$ | 149.7 | 149.54 | 11.5 | 13.39 |
| $2p^5 3s(^1P)5d\ ^2P_{3/2}$ | | 150.22 | | 7.00 |
| | 150.3 | | 14.2 | |
| $2p^5 3s(^1P)5d\ ^2D_{3/2}$ | | 150.37 | | 13.15 |
| $2p^5 3s(^1P)5d\ ^2P_{1/2}$ | 151.0 | 150.39 | 23.8 | 15.57 |
| $2s^1 3s(^1S)3p\ ^2P_{1/2}$ | | 154.63 | | 6.16 |
| | 153.0 | | 18.6 | |
| $2s^1 3s(^1S)3p\ ^2P_{3/2}$ | | 154.72 | | 12.59 |
| $2s^1 3s(^3S)3p\ ^2P_{1/2}$ | | 159.73 | | 1.09 |
| $2s^1 3s(^3S)3p\ ^2P_{3/2}$ | | 159.76 | | 1.89 |

transitions from the $2s^1 2p^6 3s^2$ and $2s^1 2p^6 3s 3p$ configurations is higher in the case of the $S^{5+}$-He system.

The excited $2s^1 3snl$ configurations with $n > 3$ decay mainly via the Coster-Kronig channel to one of the final states associated with the $2p^5 3s$ configuration. In the case of the excited $S^{5+}$ ion the Coster-Kronig channel is open also for the decay of the $2s^1 2p^6 3s 3d$ configuration. That is why the Auger lines from the $2s^1 2p^6 3s 3d$ configuration cannot be seen in the $S^{5+}$ spectrum although they are rather intensive for $Ar^{7+}$.

In a first approximation one should expect that only doublet states are populated by excitation to bound states since a spin flip is not to be expected via the Coulomb interaction. Higher spin states are populated only because they are mixed with doublet states due to the spin-orbit interaction. The states of the $2p^5 3sns$ and $2p^5 3snd$ as

well as those of the $2s^1 3snp$ ($n > 2$) configurations are excited by a dipole-allowed excitation process, while the $2p^5 3snp$, $2s3sns$, and $2s3snd$ configurations are populated via dipole-forbidden transitions, primarily via monopole or quadrupole excitation. Dipole excitation populates most probably states $^2P_{1/2}$ and $^2P_{3/2}$, monopole excitation produces the state $^2S_{1/2}$, while the quadrupole process creates predominantly the $^2D_{3/2}$ and $^2D_{5/2}$ states.

The most probable excitation process is the dipole excitation, so the most significant group of lines stems from the states of the $2p^5 3s3d$ configuration. Similarly, the dipole excited lines from the $2p^5 3s4d$ configuration are more intensive than the others in their neighborhood. The most intensive line in the low-transition-energy region is the $^2S_{1/2}$ state of the $2p^5 3s3p$ configuration produced via monopole excitation. The other states of the same configuration at the small kinetic energy side of this line are due to the decay of states populated by quadrupole excitation of a $2p$ electron. Similarly, the different states of the other $2p^5 3snp$ configurations are populated by monopole and quadrupole transitions. The monopole excitation of a $2s$ electron populates only the $2s3sns$ configuration, and its quadrupole excitation the $2s3snd$ configuration. The transitions from the $2s^1 3s3d$ configuration are rather intensive in the case of the $Ar^{7+}$ where the Coster-Kronig channel is not open for the decay of this configuration.

Configuration interaction significantly influences the population and decay of the excited states, i.e., the Auger spectrum in sodiumlike ions. The most intensive line group, i.e., the lines stemming from the decay of the $2p^5 3s3d$ configuration itself, is also massively influenced by the interaction with the doubly excited $2p^5 3p^2$ configuration. Table IV contains the squares of the expansion coefficients of this configuration in $Ar^{7+}$, while Table V shows those in $S^{5+}$. The contribution of the $2p^5 3p^2(^1D)^2P$ and $2p^5 3p^2(^3P)^2P$ states to $2p^5 3s3d(^3P)^2P_{1/2}$ is particularly high in $S^{5+}$, where their contribution is almost equal to that of all the $2p^5 3s3d$ states. The same interaction is present, but it has a somewhat smaller weight in the $Ar^{7+}$ case. This difference in the configuration interaction with the $2p^5 3p^2$ configuration is responsible for the significant difference in the structure of the $2p^5 3s3d$ configuration for the two ions. Both the line separation as well as the relative intensities differ significantly, although the atomic numbers are only slightly different.

States other than doublets (e.g., quartet states) can be excited only if they are mixed with doublet states. In the case of the $2p^5 3s3d$ configuration one can find two rather intensive transitions due to the decay of the quadruplet states $^4D_{1/2}$ and $^4D_{3/2}$. Both states have a significant mixing of doublet states of the same configuration, as can be seen in Tables IV and V.

Due to the use of the light He target, Auger transitions following double excitation contribute only negligibly to the spectrum. The small single peak found in the $Ar^{7+}$ spectrum at 164 eV kinetic energy in the projectile frame is due to the decay of the $2p^5 3p3d\ ^2D_{5/2}$ and $^2D_{3/2}$ doubly excited states of Na-like argon. Further Auger transitions from the doubly excited initial states of the $2p^5 3p^2$ configuration contribute to the spectrum between the $2p^5 3s3p\ ^2S_{1/2}$ and $2p^5 3s3d\ ^4D_{1/2}$ peaks in the case of both collision systems. The states belonging to this configuration are more strongly populated than those of the other doubly excited configurations. The reason for this enhancement is the strong configuration interaction with the $2p^5 3s3d$ singly excited configuration in the case of both ions, i.e., these states are basically populated by single excitation.

Significant configuration interaction has been found between the configurations $2p^5 3s4d$ and $2s3s3p$ in $Ar^{7+}$ (Table IV). The population expected theoretically for the $2s3s3p$ configuration taking into account this interaction is significantly smaller than that estimated without the interaction, while the population of the $2p^5 3s4d$ is correspondingly higher. A similar, but not so intensive interaction takes place between the $2s^1 3s3p$ and $2p^5 3s5d$ configurations of the $S^{5+}$ ions. A weaker interaction decreasing the intensity expected for the $2s3s^2$ configuration occurs in the $Ar^{7+}$ ion between the $2s^1 3s^2$ and $2p^5 3s4p$ configurations. The interaction between $2s^1 3s3p$ and $2p^5 3s5s$ is found to be small.

Taking into account the interaction between the above-mentioned configurations, the calculated spectrum qualitatively reproduces the structure of the experimental results for the dipole and quadrupole excitation of $2p$ electrons by He. However, for the states populated by monopole excitation it predicts a significantly smaller population than the measured one. As can be seen from Tables VI and VII, the ratios of the Auger intensities originating from the different dipole and quadrupole excited configurations are roughly in agreement with the theoretical estimate. Nevertheless, the intensities originating from the different multiplet states inside these configurations reproduce the experimental data only qualitatively (Tables II and III). Only for two dipole excited configurations, namely for $2p^5 3s^2$ and $2p^5 3s3d$, are all the Auger lines well resolved. While the ratio of the intensity of the $2p^5 3s^2\ ^2P_{3/2} - 2p^6\ ^1S_0$ transition to that of the $2p^5 3s^2\ ^2P_{1/2} - 2p^6\ ^1S_0$ coincides approximately with the theoretical prediction, the intensities of the transitions from the $2p^5 3s3d$ configuration agree with it only to within a factor of 2.

The experimentally observed relative intensities associated with transitions from states populated by monopole excitation are higher than the values estimated by means of collision strengths using the Born approximation. These collision strengths are good estimates of the experimental values for a high-energy electron-ion collision system covering a broad impact-parameter region. The observed deviation is supposed to be caused by the difference between the exciting He atom and the high-energy electron used in the model calculations. Because of the screening effect of the atomic electrons most of the excitations are due to the collisions with impact parameters smaller than the mean orbital radius of the exciting He atom. The probability of dipole excitation is higher at larger impact-parameter values, while monopole excitation is characterized primarily by small impact parameters. Hence, in a collision with a completely screened He atom, the dipole excitation is reduced relative to the

TABLE IV. Square of the expansion coefficients of intermediate coupling states specified by the total angular momentum and the largest eigenvector component present in the given configuration of $Ar^{7+}$. Contributions smaller than 0.01 are neglected.

| State | Energy (eV) | $2p^5 3s^2$ $(^1S)^2P$ | $2p^5 3s3d$ $(^3P)^4F$ | $2p^5 3s3d$ $(^3P)^4D$ | $2p^5 3s3d$ $(^3P)^4P$ | $2p^5 3s3d$ $(^1P)^2D$ | $2p^5 3s3d$ $(^3P)^2D$ | $2p^5 3s3d$ $(^1P)^2P$ | $2p^5 3s3d$ $(^3P)^2P$ | $2p^5 3p^2$ $(^1D)^2D$ | $2p^5 3p^2$ $(^3P)^2P$ | $2p^5 3p^2$ $(^1D)^2P$ | $2p^5 3p^2$ $(^1S)^2P$ | $2p^5 3d^2$ (all) | $2s^1 3s3p$ $(^3S)^2P$ |
|---|---|---|---|---|---|---|---|---|---|---|---|---|---|---|---|
| $2p^5 3s^2$ | | | | | | | | | | | | | | | |
| $(^1S)^2P_{3.2}$ | 100.18 | 0.97 | | | | | | | | | 0.03 | | | | |
| $(^1S)^2P_{1/2}$ | 102.31 | 0.97 | | | | | | | | | 0.03 | | | | |
| $2p^5 3s3d$ | | | | | | | | | | | | | | | |
| $(^3P)^4D_{1/2}$ | 142.65 | | | 0.81 | | | | 0.09 | 0.02 | | | 0.01 | 0.07 | | |
| $(^3P)^4D_{3/2}$ | 142.79 | | 0.07 | 0.58 | 0.01 | 0.02 | 0.01 | 0.21 | | | 0.05 | | 0.04 | | |
| $(^1P)^2P_{3/2}$ | 143.57 | | 0.10 | 0.21 | 0.01 | 0.07 | 0.05 | 0.21 | 0.04 | 0.01 | 0.20 | | 0.09 | 0.01 | |
| $(^1P)^2D_{3/2}$ | 144.03 | | 0.10 | 0.02 | 0.02 | 0.48 | 0.19 | 0.03 | 0.03 | | 0.10 | | 0.03 | | |
| $(^1P)^2P_{3/2}$ | 146.22 | | | 0.04 | 0.01 | 0.01 | 0.01 | 0.42 | 0.26 | | 0.15 | 0.06 | 0.03 | | |
| $(^1P)^2P_{1/2}$ | 146.33 | | | 0.06 | | | | 0.51 | 0.16 | | 0.14 | 0.07 | 0.04 | | |
| $(^1P)^2D_{3/2}$ | 148.78 | | | | | 0.19 | 0.36 | | 0.14 | 0.14 | 0.06 | 0.09 | | 0.01 | |
| $(^3P)^2P_{1/2}$ | 149.30 | | | | | | | | 0.60 | | 0.12 | 0.25 | | 0.01 | 0.01 |
| $(^3P)^2P_{3/2}$ | 150.81 | | | | | 0.08 | 0.15 | 0.02 | 0.40 | 0.06 | 0.08 | 0.19 | | 0.01 | 0.01 |

| State | Energy (eV) | $2p^5 3s^2$ $(^1S)^2P$ | $2p^5 3s3d$ $(^3P)^4D$ | $2p^5 3s3d$ $(^3P)^4P$ | $2p^5 3s3d$ $(^3P)^2D$ | $2p^5 3s3d$ $(^1P)^2P$ | $2p^5 3s3d$ $(^3P)^2P$ | $2p^5 3p^2$ $(^3P)^4D$ | $2p^5 3p^2$ $(^3P)^4P$ | $2p^5 3p^2$ $(^3P)^4S$ | $2p^5 3p^2$ $(^1D)^2D$ | $2p^5 3p^2$ $(^3P)^2P$ | $2p^5 3p^2$ $(^1D)^2P$ | $2p^5 3p^2$ $(^1S)^2P$ | $2p^5 3d^2$ (all) |
|---|---|---|---|---|---|---|---|---|---|---|---|---|---|---|---|
| $2p^5 3p^2$ | | | | | | | | | | | | | | | |
| $(^1D)^2P_{1/2}$ | 132.39 | | | | | 0.05 | 0.07 | 0.01 | 0.04 | | | 0.24 | 0.56 | 0.01 | |
| $(^1S)^2P_{1/2}$ | 141.13 | | 0.01 | | | 0.16 | 0.10 | 0.01 | | | | 0.31 | 0.04 | 0.35 | |
| $(^1S)^2P_{1/2}$ | 143.86 | | 0.11 | | | 0.17 | 0.04 | | | | | 0.17 | | 0.47 | 0.02 |
| $(^1D)^2P_{3/2}$ | 132.64 | | | | 0.01 | 0.03 | 0.04 | 0.03 | 0.25 | | 0.04 | 0.19 | 0.38 | 0.02 | |
| $(^3P)^4P_{3.2}$ | 133.36 | | | | 0.01 | 0.01 | 0.02 | 0.02 | 0.64 | 0.06 | 0.03 | 0.05 | 0.15 | | |
| $(^1S)^2P_{3.2}$ | 140.04 | 0.02 | | 0.01 | | 0.04 | 0.05 | | | | 0.01 | 0.07 | 0.06 | 0.71 | 0.02 |

| State | Energy (eV) | $2p^5 3s5s$ $(^1P)^2P$ | $2p^5 3s5s$ $(^3P)^2P$ | $2p^5 3s4d$ $(^3P)^4D$ | $2p^5 3s4d$ $(^1P)^2D$ | $2p^5 3s4d$ $(^1P)^2P$ | $2p^5 3s4d$ $(^3P)^2P$ | $2s^1 3s3p$ $(^1S)^2P$ | $2s^1 3s3p$ $(^3S)^2P$ |
|---|---|---|---|---|---|---|---|---|---|
| $2s^1 3s3p$ | | | | | | | | | |
| $(^1S)^2P_{1/2}$ | 196.58 | | | 0.02 | | 0.13 | 0.10 | 0.48 | 0.25 |
| $(^3S)^2P_{1/2}$ | 202.41 | 0.01 | | | | | 0.35 | 0.62 | |
| $(^1S)^2P_{3/2}$ | 196.68 | | | 0.01 | 0.01 | 0.07 | 0.09 | 0.50 | 0.30 |
| $(^3S)^2P_{3/2}$ | 202.45 | 0.01 | 0.01 | | | | 0.38 | 0.58 | |

TABLE V. Square of the expansion coefficients of intermediate coupling states specified by the total angular momentum and the largest eigenvector component present in the given configuration of $S^{5+}$.

| State | Energy (eV) | $2p^5 3s^2$ $(^1S)^2P$ | $2p^5 3s3d$ $(^3P)^4F$ | $2p^5 3s3d$ $(^3P)^4D$ | $2p^5 3s3d$ $(^3P)^4P$ | $2p^5 3s3d$ $(^1P)^2D$ | $2p^5 3s3d$ $(^3P)^2D$ | $2p^5 3s3d$ $(^1P)^2P$ | $2p^5 3s3d$ $(^3P)^2P$ | $2p^5 3p^2$ $(^1D)^2D$ | $2p^5 3p^2$ $(^3P)^2P$ | $2p^5 3p^2$ $(^1D)^2P$ | $2p^5 3p^2$ $(^1S)^2P$ | $2p^5 3d^2$ (all) | $2s^1 3s3p$ $(^3S)^2P$ |
|---|---|---|---|---|---|---|---|---|---|---|---|---|---|---|---|
| $2p^5 3s^2$ | | | | | | | | | | | | | | | |
| $(^1S)^2P_{3/2}$ | 75.79 | 0.97 | | | | | | | | | 0.03 | | | | |
| $(^1S)^2P_{1/2}$ | 76.68 | 0.97 | | | | | | | | | 0.03 | | | | |
| $2p^5 3s3d$ | | | | | | | | | | | | | | | |
| $(^3P)^4D_{1/2}$ | 107.69 | | | 0.89 | | | | 0.06 | 0.02 | | | | 0.03 | | |
| $(^3P)^4D_{3/2}$ | 107.78 | | 0.08 | 0.79 | 0.02 | 0.02 | 0.01 | 0.08 | 0.01 | | 0.01 | | 0.01 | | |
| $(^1P)^2D_{3/2}$ | 108.49 | | 0.08 | 0.03 | | 0.38 | 0.19 | 0.19 | | 0.01 | 0.07 | | 0.05 | | |
| $(^1P)^2D_{3/2}$ | 108.78 | | 0.02 | 0.05 | 0.01 | 0.24 | 0.08 | 0.23 | 0.03 | | 0.21 | | 0.12 | 0.01 | |
| $(^3P)^2P_{3/2}$ | 110.05 | | | 0.03 | 0.01 | 0.01 | 0.01 | 0.32 | 0.38 | | 0.16 | 0.03 | 0.05 | | |
| $(^1P)^2P_{1/2}$ | 110.16 | | | 0.04 | | | | 0.40 | 0.32 | | 0.13 | 0.02 | 0.07 | | |
| $(^3P)^2D_{3/2}$ | 112.85 | | | | | 0.21 | 0.38 | 0.01 | 0.08 | 0.17 | 0.06 | 0.08 | | 0.02 | |
| $(^3P)^2P_{1/2}$ | 113.25 | | | | | | | 0.05 | 0.45 | | 0.17 | 0.31 | | 0.01 | 0.01 |
| $(^3P)^2P_{3.2}$ | 114.09 | | | | | 0.06 | 0.11 | 0.05 | 0.35 | 0.05 | 0.11 | 0.24 | | 0.01 | 0.01 |

| State | Energy (eV) | $2p^5 3s^2$ $(^1S)^2P$ | $2p^5 3s3d$ $(^3P)^4D$ | $2p^5 3s3d$ $(^3P)^4P$ | $2p^5 3s3d$ $(^3P)^2D$ | $2p^5 3s3d$ $(^1P)^2P$ | $2p^5 3s3d$ $(^3P)^2P$ | $2p^5 3p^2$ $(^3P)^4D$ | $2p^5 3p^2$ $(^3P)^4P$ | $2p^5 3p^2$ $(^3P)^4S$ | $2p^5 3p^2$ $(^1D)^2D$ | $2p^5 3p^2$ $(^3P)^2P$ | $2p^5 3p^2$ $(^1D)^2P$ | $2p^5 3p^2$ $(^1S)^2P$ | $2p^5 3d^2$ (all) |
|---|---|---|---|---|---|---|---|---|---|---|---|---|---|---|---|
| $2p^5 3p^2$ | | | | | | | | | | | | | | | |
| $(^1D)^2P_{1/2}$ | 100.07 | | | | | 0.05 | 0.08 | 0.01 | 0.02 | | | 0.24 | 0.58 | 0.01 | |
| $(^1S)^2P_{1/2}$ | 106.71 | 0.01 | 0.01 | | | 0.12 | 0.09 | | | | | 0.28 | 0.04 | 0.42 | 0.01 |
| $(^1S)^2P_{1.2}$ | 108.86 | 0.01 | 0.06 | | | 0.31 | 0.02 | | | | | 0.18 | | 0.40 | 0.02 |
| $(^1D)^2P_{3/2}$ | 100.28 | | | | 0.01 | 0.04 | 0.06 | 0.01 | 0.14 | | 0.03 | 0.22 | 0.46 | 0.02 | |
| $(^3P)^4P_{3.2}$ | 100.80 | | | | | 0.01 | 0.01 | 0.02 | 0.79 | 0.03 | 0.01 | 0.03 | 0.09 | | |
| $(^1S)^2P_{3.2}$ | 106.10 | 0.02 | | | | 0.05 | 0.06 | | | | | 0.10 | 0.06 | 0.68 | 0.03 |

TABLE VI. Comparison of the calculated (CIHF code) and measured relative Auger intensities in the decay of an excited $Ar^{7+}$ ion. The total intensities are normalized to 1000.

| Configuration | Intensity Expt. | Intensity Theory | Expt;theory ratio | Mode of excitation |
|---|---|---|---|---|
| $2p^5 3s^2$ | 23.66 | 33.55 | 0.71 | dipole |
| $2p^5 3s 3p$ | 17.59 | 15.43 | 1.14 | quadrupole |
| | 121.61 | 44.58 | 2.73 | monopole |
| $2p^5 3s 3d$ | 571.33 | 612.81 | 0.93 | dipole |
| $2p^5 3s 4s$ | 14.81 | 3.88 | 3.82 | dipole |
| $2p^5 3s 4p$ | ? | 2.85 | | quadrupole |
| | 27.50 | 14.06 | 1.96 | monopole |
| $2p^5 3s 4d$ | 97.71 | 150.49 | 0.65 | dipole |
| $2p^5 3s 5s$ | ? | 0.86 | | dipole |
| $2p^5 3s 5p$ | ? | 2.35 | | quadrupole |
| | 8.31 | 5.14 | | monopole |
| $2p^5 3s 5d$ | 36.58 | 62.55 | 0.58 | dipole |
| $2s^1 3s^2$ | ? | 3.54 | | monopole |
| $2s^1 3s 3p$ | 13.96 | 10.62 | 1.31 | dipole |
| $2s^1 3s 3d$ | 40.67 | 23.93 | 1.70 | quadrupole |
| $2p^5 3p^2$ | 26.21 | 11.53 | 2.27 | double exc.: dipole (+monopole) |

monopole transitions.

The excitation cross sections for the two collision systems were calculated also by a simple PWBA code [13] based on the method of Bates and Griffing [14]. Scaled hydrogenlike wave functions for the projectile and screened target potential were used in the calculations. The values obtained for the ratio of cross sections due to the monopole excitation to those produced by dipole transitions are found to be 0.19 in the $Ar^{7+}$-He and 0.22 in the case of the $S^{5+}$-He collision system. These data agree with the experimental values for the systems $Ar^{7+}$-He (0.19) and $S^{5+}$-He (0.23). The value obtained by the same calculation without target screening was found to be 0.10 for both cases, which deviates significantly from the experimental values. This result supports the conclusion drawn in the preceding paragraph, namely, that the presence of screening electrons in the target atom reduces the dipole excitation relative to the monopole transitions.

A comparison of the model spectrum with the experimental $Ar^{7+}$ $L$ Auger spectra obtained at collisions with heavier targets shows that in these cases (Table VIII) the ratio of monopole to dipole excitation agrees with the PWBA prediction calculated by the Cowan [10] program.

TABLE VII. Comparison of the calculated (CIHF code) and measured relative Auger intensities in the decay of an excited $S^{5+}$ ion. The total intensities are normalized to 1000.

| Configuration | Intensity Expt. | Intensity Theory | Expt;theory ratio | Mode of excitation |
|---|---|---|---|---|
| $2p^5 3s^2$ | 36.05 | 43.39 | 0.83 | dipole |
| $2p^5 3s 3p$ | 21.91 | 16.57 | 1.33 | quadrupole |
| | 121.07 | 46.04 | 2.63 | monopole |
| $2p^5 3s 3d$ | 466.93 | 563.39 | 0.83 | dipole |
| $2p^5 3s 4s$ | 9.62 | 5.37 | 1.79 | dipole |
| $2p^5 3s 4p$ | 14.74 | 2.00 | 7.37 | quadrupole |
| | 25.88 | 11.12 | 2.33 | monopole |
| $2p^5 3s 4d$ | 141.42 | 145.41 | 0.90 | dipole |
| $2p^5 3s 5s$ | ? | 1.88 | | dipole |
| $2p^5 3s 5p$ | ? | 0.98 | | quadrupole |
| | 8.71 | 11.58 | 0.75 | monopole |
| $2p^5 3s 5d$ | 85.38 | 87.06 | 0.98 | dipole |
| $2s^1 3s^2$ | 23.31 | 5.37 | 4.34 | monopole |
| $2s^1 3s 3p$ | 18.55 | 21.74 | 0.85 | dipole |
| $2p^5 3p^2$ | 26.40 | 25.42 | 1.04 | double exc.: dipole (+monopole) |

TABLE VIII. Comparison of the expected (CIHF code) and measured relative Auger intensities in the decay of Na-like Ar and S ions singly excited by high-energy collisions with different targets. The ratio of the experimental to the theoretical relative intensities is shown.

| Excitation | 110-MeV $Ar^{7+}+He$ | 64-MeV $S^{5+}+He$ | 174-MeV $Ar^{7+}+He$ | 137-MeV $Ar^{7+}+Ar$ |
|---|---|---|---|---|
| $2p$ monopole | 2.47 | 2.26 | 1.12 | 0.80 |
| $2p$ dipole | 0.85 | 0.86 | 0.91 | 0.92 |
| $2p$ quadrupole | 1.14 | 1.33 | | |
| $2s$ monopole | | 4.34 | | |
| $2s$ dipole | 1.31 | 0.98 | | |
| $2s$ quadrupole | 1.70 | | 2.10 | 1.80 |

In this case the result deviates from the value obtained by the Bates-Griffing PWBA with screening. There are two significant differences in comparison with the case of excitation by He atoms. First, the effect of the atomic electrons is relatively high, i.e., a rather large part of the effective impact-parameter region is characterized by the presence of the electrons. Second, the charge of the target is much higher. For high target charges one should expect deviations from the perturbation theoretical approach [15]. The high target charge has different effects. First, at high Coulomb fields a saturation effect occurs [15], therefore the measured cross sections are smaller than those predicted by perturbation theory. For the screened heavy target this saturation is expected to decrease first of all the intensity due to collisions at small impact parameters, i.e., the monopole excitation. Because of the high target charge the role of multiple processes is higher, so configurations which are produced by pure single excitation via He impact can be created also by multiple processes, such as ionization and simultaneous capture. An indication of the presence of this latter double process is the relative increase of the intensity from the $2p^5 3s^2$ configuration in the $Ar^{7+}$-Ar collision system. Moreover, the role of multipole excitation is higher in these cases.

## SUMMARY

The $L$ Auger spectrum emitted in the collisions of high-energy sodiumlike argon and sulfur ions with He atoms has been measured with high resolution. The spectrum has been reproduced by transition-energy and intensity values calculated by using the configuration-interaction Hartree-Fock code by Cowan [10]. From the comparison of the measured and calculated transition energies and intensities the following conclusions can be drawn.

The measured spectrum is due to the decay of configurations produced by monopole, dipole, and quadrupole excitation of both $2p$ and $2s$ electrons. The structure of the excited ions and the population and decay of the states produced in these collisions are strongly influenced by the mixing of different multiplet states and by configuration interaction. The most striking example is the strong interaction between the $1s^2 2p^5 3s 3d$ and $1s^2 2s^2 2p^5 3p^2$ configurations in both ions. As a consequence of this interaction there is an intensive $2p^5 3p^2$ contribution to the spectrum. The difference in the structure of the line group due to the decay of the $2p^5 3s 3d$ configuration in the two ions is also due to the different strength of this interaction in the two ions. The pronounced $2p$-$2s$ interaction between the $2p^5 3s 4d$ and $2s^1 2p^6 3s 3p$ configurations in the $Ar^{7+}$ ion is also remarkable.

The screening effect of the atomic electrons appears to be responsible for the deviation of the ratio of the intensities due to different multipole excitations from the PWBA estimate using a bare Coulomb interaction potential.

## ACKNOWLEDGMENTS

Thanks are due to Dr. S. Ricz and Dr. B. Sulik for useful discussions. The excellent technical assistance of U. Stettner is also acknowledged.

*Permanent address: Institute of Nuclear Research of the Hungarian Academy of Science, H-4001 Debrecen, Postafiók 51, Hungary.

†Present address: Department of Chemistry and Physics, Middle Tennessee State University, Murfreesboro, TN 37132.

‡Present address: ISMRA, Laboratoire de Spectroscopie Atomique, F-14032 Caen, France.

[1] A. Itoh, T. Schneider, G. Schiwietz, Z. Roller, H. Platten, G. Nolte, D. Schneider, and N. Stolterfoht, J. Phys. B **16**, 3965 (1983).

[2] A. Itoh, D. Schneider, T. Schneider, T. J. M. Zouros, G. Nolte, G. Schiwietz, W. Zeitz, and N. Stolterfoht, Phys. Rev. A **31**, 684 (1985).

[3] N. Stolterfoht, Phys. Rep. **146**, 315 (1987).

[4] R. Hutton, M. H. Prior, S. Chantrenne, Mau Hsiung

Chen, and D. Schneider, Phys. Rev. A **39**, 4902 (1989).
[5] A. Bordenave-Montesquieu, P. Benoit-Cattin, M. Boudjema, A. Gleizes, and S. Dousson, Nucl. Instrum. Methods B **23**, 94 (1987).
[6] D. J. Pegg, H. H. Haselton, R. S. Thoe, P. M. Griffin, M. D. Brown, and I. A. Sellin, Phys. Rev. A **12**, 1330 (1975).
[7] F. Folkmann, M. Cramon, R. Mann, and H. F. Beyer, Phys. Scr. **73**, 166 (1983).
[8] D. Schneider, M. H. Chen, S. Chantrenne, R. Hutton, and M. H. Prior, Phys. Rev. A **40**, 4313 (1989).
[9] D. Schneider, P. Beiersdorfer, M. Chen, R. Walling, J. D. Molitoris, and D. DeWitt, Phys. Rev. A **40**, 181 (1989).
[10] R. D. Cowan, *The Theory of Atomic Structure and Spectra* (University of California Press, Berkeley, 1981).
[11] T. Matsuo, J. Urakawa, A. Yagishita, Y. Awaya, T. Kambara, M. Kase, and H. Kumagai, J. Phys. B **16**, L239 (1983).
[12] R. D. Cowan, Ref. [10], p. 568, Eq. 18.157.
[13] G. Schiwietz, D. Schneider, and J. Tanis, Phys. Rev. Lett. **59**, 1561 (1987).
[14] D. R. Bates and G. Griffing, Proc. Phys. Soc. London **26**, 961 (1953).
[15] B. Brendlé, R. Gayet, J. P. Rozet, and K. Wohrer, Phys. Rev. Lett. **54**, 2007 (1985).